Differential Distortion of Substrate Occurs When It Binds to DNA Photolyase: A 2-Aminopurine Study†

Kongsheng Yang and Robert J. Stanley*

Department of Chemistry, Temple University, 201 Beury Hall, Philadelphia, Pennsylvania 19122

Received March 1, 2006; Revised Manuscript Received June 9, 2006

ABSTRACT: Cyclobutylpyrimidine dimers (CPDs) are formed between adjacent pyrimidines in DNA when it is exposed to ultraviolet light. CPDs can be directly repaired by DNA photolyase (PL) upon absorption of blue-green light. We have used the fluorescent adenine analogue 2-aminopurine (2Ap) to probe the local double-helical structure of the DNA substrate when it binds to the protein. Duplex melting temperatures and van't Hoff enthalpies were obtained by both UV−vis absorption and fluorescence spectroscopies to ascertain the effect of the probe and CPD on DNA stability. Steady-state fluorescence measurements of the single- and double-stranded oligos showed that the local region around the 5′-side of the CPD lesion was more disrupted and destacked than the 3′-side in substrate−protein complexes. These results were compared with those of a protein−substrate crystal structure, demonstrating that the crystal structure and solution-state studies are in agreement with regard to the differential distortions of the target DNA at the active site of the protein.

When DNA is exposed to UV light, a variety of photoproducts are produced (*1*). The major photoproduct (*2*, *3*) is the cyclobutylpyrimidine dimer (CPD),[1] which is formed between two adjacent pyrimidines. If left unrepaired, these photoproducts lead to mutagenesis and cell death (*4*−*6*). There are several enzymatic pathways (*7*−*9*) for repairing such damage. One of them is direct repair through photoinduced electron transfer by DNA photolyase (*10*).

DNA photolyase is a 54 kDa monomeric protein containing two chromophores (*11*). One is the catalytic cofactor flavin adenine dinucleotide (FAD), and the second chromophore is either methenyltetrahydrofolate or deazaflavin. There are three possible oxidation states for FAD inside DNA photolyase: oxidized FAD, one-electron-reduced semiquinone ($FADH^{\bullet}$), and the anionic two-electron-reduced hydroquinone ($FADH^{-}$). Only the fully reduced form is capable of repair, but the protein can bind substrate in all three oxidation states with approximately the same affinity (*2*, *10*). Excitation of $FADH^{-}$ with blue-green light results in ultrafast electron transfer, leading to the repair of the CPD (*12*−*15*).

In general, DNA-binding proteins exhibit a wide variety of binding motifs to accommodate their DNA substrate. Base flipping (*16*) is one such motif that appears in several different functional classes, including methyltransferases (*17*) and endonucleases (*18*). On the basis of the first crystal structure of the photolyase protein (without substrate), it was believed that base flipping of the CPD out of the DNA double helix was required to bring the CPD and $FADH^{-}$ close enough for efficient electron transfer (*19*).

Scheme 1

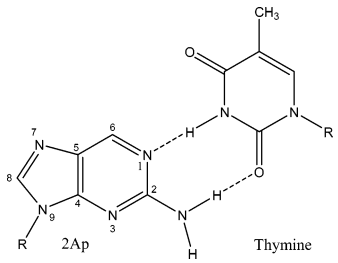

This hypothesis was corroborated by several studies (*20*, *21*), including one from our own laboratory (*22*) which suggested that base flipping was accompanied by a large change in the local structure of the DNA duplex around the 3′-side of the lesion. Our approach utilized 2-aminopurine (2Ap; see Scheme 1), an adenine analogue (*23*) whose fluorescence quantum yield is sensitive to changes in base stacking. 2Ap has been used widely to study protein−nucleic acid interactions (*18*, *24*, *25*). In our study, 2Ap was incorporated into the substrate duplex with the analogue opposing the 3′-thymine of the CPD on the complementary strand. The fluorescence quantum yield of this probe increased by a factor of more than 3 compared to the yield of the CPD-containing duplex DNA in the absence of PL_{ox}, suggesting that disruption of base stacking on the complementary strand takes place upon substrate binding.

In this paper, we explore structural perturbations surrounding the CPD and its complementary adenines across the helix. We present evidence of a much larger distortion at the 3′-side versus the 5′-side of the complementary strand due to

† We gratefully acknowledge support from the National Science Foundation Division of Molecular and Cellular Biosciences (Grant MCB 0347087).

* To whom correspondence should be addressed: Department of Chemistry, Temple University, 201 Beury Hall, Philadelphia, PA 19122. Telephone: (215) 204-2027. Fax: (215) 204-1532. E-mail: rstanley@temple.edu.

[1] Abbreviations: CPD, cyclobutylpyrimidine dimer; 2Ap or A, 2-aminopurine; PL_{ox}, oxidized DNA photolyase; FAD_{ox}, oxidized FAD; $FADH^{\bullet}$, semiquinone FAD; $FADH^{-}$, reduced anionic FAD hydroquinone.

10.1021/bi060408u CCC: $33.50
Published on Web 08/22/2006

base flipping in vitro, in agreement with the recently determined crystal structure (*26*).

EXPERIMENTAL PROCEDURES

Protein and Substrate. Escherichia coli DNA photolyase was prepared as described in ref *27*. The protein was depleted of both chromophores and reconstituted with oxidized FAD. Double reverse phase HPLC-purified 11-mer oligonucleotides were purchased from Integrated DNA Technologies. All oligonucleotides were resuspended in HPLC-grade water and used without further purification, except for the CPD-containing strand. The CPD-containing oligonucleotide was generated as described by Banerjee et al. (*28*).

Steady-State Fluorescence Emission Spectra. Fluorescence emission spectra were obtained using a SPEX FluoroMax-2 fluorimeter. Emission spectra for 2Ap-containing samples were obtained from 330 to 510 nm with excitation at 317 nm. The scans were taken with an integration time of 0.2 s, a step size of 2 nm, and excitation and emission band-passes of 8 and 4 nm, respectively. Four replicates of each emission spectrum were averaged together. The excitation and emission light were unpolarized. Spectra were corrected for the background fluorescence and Raman scattering of the buffer or control sample and corrected for both the excitation and emission wavelength bias of the fluorimeter. A 0.40 cm × 1.0 cm fluorescence quartz cell was used. The fluorimeter cuvette holder was cooled by a variable-temperature circulating water bath. The cuvette was allowed to equilibrate in the holder for 10 min in the dark prior to a scan.

Samples were prepared freshly for each scan. Mixtures of oligonucleotides were placed in a sterile Eppendorf tube in a minimal volume, typically less than 50 μL. These samples were heated in a 75−80 °C water bath for 10 min and allowed to cool to room temperature on the laboratory bench for at least 30 min. If appropriate, PL_{ox} was added, and the samples were then brought to a total volume of 1 mL in buffer [50 mM potassium phosphate, 100 mM potassium chloride, 0.1 mM EDTA, and 10 mM β-mercaptoethanol (pH 7.5)]. The fluorescence cuvette containing the sample was sonicated briefly in a small ultrasonic bath to remove bubbles before each measurement. All measurements were taken at 15.0 ± 0.1 °C.

Melting Temperature Measurements. Both fluorescence emission and absorbance methods were used to determine the melting point of the duplexes. A constant-wavelength analysis as a function of temperature was performed with excitation at 317 nm and emission at 370 nm for 2Ap-containing samples. The fluorimeter cuvette holder was connected to a variable-temperature circulating water bath set to 10 °C. To obtain a melting curve, the temperature controller was set to 85 °C and spectra were recorded at 15 s intervals with a temperature change of ~2 °C/min. The sample temperature inside the cuvette was monitored using a thermocouple (OMEGA k type HH22). The average of three heating profiles was fitted to a fifth-order polynomial to obtain the temperature scale as a function of time. Each melting curve was repeated in triplicate.

For the absorbance method, samples were prepared as described above. Absorbance spectra were obtained using a Hewlett-Packard HP8452A diode array spectrophotometer, having a resolution of 2 nm. Absorbance spectra were measured by using the time-based kinetics mode of the spectrometer. Absorbance data were taken from 240 to 420 nm with an integration time of 2 s. The absorbance from 240 to 280 nm was baseline-corrected by subtracting the average absorbance from 400 to 420 nm. A 0.10 cm × 1.0 cm quartz cell with black walls was used. The cuvette was allowed to equilibrate in the holder for 10 min prior to a scan. The temperature axis was calibrated as described above.

Melting points, T_m, were obtained from the zero crossing of the numerical first derivative of the melting curves. In addition, the melting point curves were analyzed to obtain estimates of the van't Hoff transition enthalpy, ΔH_{vH}, according to the method of Breslauer (*29*), where the enthalpy of melting is related to the slope of the melting curve at the temperature at which one-half of the duplexes have melted:

$$\Delta H_{vH} = 6RT_m^2\left(\frac{\partial \alpha}{\partial T}\right)_{T_m} \quad (1)$$

where α is the fraction of unmelted duplexes, T_m is the temperature at which $\alpha = 0.5$, and R is the gas constant. This analysis assumes that duplex dissociation occurs in an "all-or-nothing" manner and is not applicable to cases where there are more than two states (folded and unfolded).

RESULTS

Melting Temperatures of Probe-Containing Duplexes. The oligonucleotides used in this study were as follows:

5'-GCAAGTTGGAG-3'	T-T
5'-GCAAGT<>TGGAG-3'	T<>T or CPD
5'-CTCCAACTTGC-3'	A-A
5'-CTCCA<u>A</u>CTTGC-3'	3'-2Ap
5'-CTCC<u>A</u>ACTTGC-3'	5'-2Ap

where T-T stands for the complementary strand, T<>T indicates the cyclobutylpyrimidine dimer-containing oligonucleotide (CPD), and <u>A</u> shows the position of the fluorescent base analogue in the 2Ap-containing ssDNA.

Control experiments were performed to determine the ratio of ss complement to ss probe concentrations necessary to achieve maximal fluorescence quenching. For example, the normalized fluorescence intensity at 370 nm versus the [T-T]/[3′-2Ap] or [CPD]/[3′-2Ap] ratio was plotted to determine the saturation concentration of the 3′-2Ap probe for its opposing strand [Figure 1, (△) 3′-2Ap/T-T and (□) 3′-2Ap/CPD]. A ratio of ~1.4 was found for both the CPD and the T-T oligos for 2Ap. This ratio was maintained in all subsequent experiments.

Panels a and b of Figure 2 show the melting profiles of 2Ap-containing duplexes by both absorbance and fluorescence methods. The data have been baseline-corrected and normalized to unity. These data report on the thermodynamic destabilization introduced when an adenine is replaced by the analogue, and when the T-T tract is replaced by the CPD substrate. The concentration of the 2Ap oligo was 0.50 and

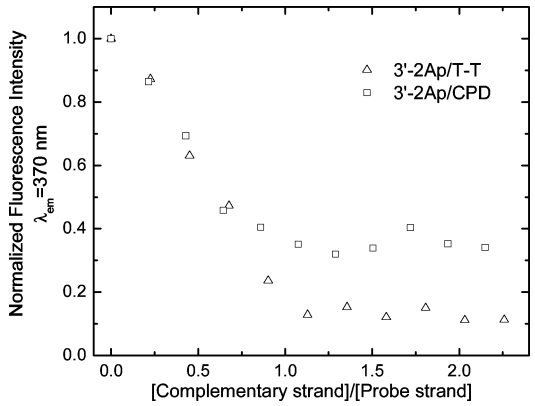

FIGURE 1: Titration curve between the 3′-2Ap probe strand and either the CPD or T-T complementary strand at room temperature and 150 mM salt. The fluorescence intensity at 370 nm was normalized to the fluorescence intensity of the probe strand at zero complementary strand concentration.

Table 1: Melting Temperatures of Duplexes

	T_m ($\pm\sigma$) (°C)			
	fluorescence		absorbance	
	T-T	CPD	T-T	CPD
A-A	–	–	45.0 (0.5)	37.0 (0.5)
3′-2Ap	40.3 (0.9)	33.2 (0.5)	42.8 (1.0)	33.3 (1.2)
5′-2Ap	42.5 (0.5)	39.2 (0.5)	44.1 (0.5)	39.3 (0.9)

0.25 μM for absorption and fluorescence runs, respectively. The concentration of the T-T oligo was 0.70 and 0.35 μM for absorption and fluorescence, respectively. The concentration of the T<>T oligo was 0.90 and 0.60 μM for absorption and fluorescence, respectively. The K^+ concentration was 0.11 M for the absorption experiments and 0.15 M for the fluorescence experiments. Also shown are the absorption melting profiles for the control duplexes, which do not contain 2Ap ([A-A] = 0.50 μM, [T-T] = 0.70 μM, [T<>T] = 0.90 μM, and [K^+] = 0.11 M).

As shown in Table 1, the inclusion of the 2Ap probe at the 5′-position in a duplex without the CPD lowers the T_m by ~1 °C compared to that of the control duplex (no probe and no CPD), as determined by UV absorption spectroscopy. However, 2Ap at the 3′-position depresses the melting temperature by ~2 °C.

Inclusion of the CPD on the opposing strand lowers the T_m further. The control (A-A) strand annealed to the CPD strand melts at a temperature ~8 °C lower than that of a duplex without the CPD. Similarly, the T_m of the 3′-2Ap/CPD duplex is suppressed by ~10 °C and that of the 5′-2Ap/CPD strand lowered by 5 °C relative to those of their nonlesion counterparts.

Although the T_m values as determined using fluorescence are generally lower than those measured by UV−vis absorption spectroscopy, the difference in melting points between 3′-2Ap/T-T and 5′-2Ap/T-T duplexes is very similar to that obtained by the absorbance measurement. Interestingly, this is not the case when the CPD-containing strand is introduced: both 3′-2Ap/CPD and 5′-2Ap/CPD duplexes have the same melting point, ~33 and ~39 °C, respectively. This suggests that destacking introduced by the CPD dominates the effect on the melting point, and therefore duplex stability, more so than the introduction of the 2Ap analogue.

Table 2: ΔH_{vH} (T_m) Values for Duplexes

	ΔH_{vH} (kcal/mol) [T_m (°C)]			
	fluorescence		absorbance	
	T-T	CPD	T-T	CPD
A-A	–	–	−94 (44.5)	−82 (36.2)
3′-2Ap	−85 (39.3)	−81 (32.9)	−99 (42.4)	−78 (33.4)
5′-2Ap	−96 (41.2)	−95 (38.7)	−106 (43.9)	−95 (39.0)

van't Hoff Enthalpies. The enthalpies for melting, ΔH_{vH}, were determined for each melting curve, and the values for each case are given in Table 2. This enthalpy is the heat required to dissociate the duplex into two single-stranded oligos. The tabulated values have an estimated error of ~20%. A comparison of the T_m from this approach gave the same results as the derivative method within ~0.5 °C. However, this consistency is not generally observed in the enthalpies derived from the analysis of Breslauer (*29*).

UV−vis measurements showed inclusion of 2Ap did not significantly change the ΔH_{vH} relative to those of the control duplexes. This is also consistent with the very similar melting points obtained for the three cases. However, the CPD-containing duplexes had a ca. 10−20 kcal/mol lower enthalpy than the duplexes containing no lesion. In each case, this change was mirrored in a lowering of the melting point of the CPD-containing duplex as described above. These results are consistent with the observation of Park et al. (*30*) that inclusion of a CPD in a decamer reduces the level of base stacking and hydrogen bonding in both the CPD-containing strand and the complementary strand. However, in another study, Taylor's group measured the enthalpy and entropy of decamer and dodecamer duplexes containing a CPD and showed that in both cases the CPD did not change the enthalpy significantly, despite a decrease in the melting point observed for the CPD-containing duplexes (*31*, *32*).

The most pronounced change was obtained for the 3′-2Ap/CPD duplex, which lost ~20 kcal/mol relative to the nonlesion duplex. Comparison with the crystal structure of the decamer (*30*) shows that the 5′-side of the CPD suffers a greater loss of base stacking and hydrogen bonding than the complementary strand at the 3′-side. This observation is consistent with the larger change in enthalpy measured in this study.

Generally, lower enthalpies were obtained by fluorescence. Interestingly, there was a much smaller difference in the enthalpy with the inclusion of a CPD, with the 5′-2Ap being somewhat more stable than the 3′-2Ap case. In absolute terms, the inclusion of a 2Ap base lowered the enthalpy by ~10 kcal/mol relative to the absorbance case. This suggests that the environment of the 2Ap is already disordered sufficiently that it melts at a lower temperature than the duplex as a whole, and that fluorescence is reporting on a localized change in structure.

Emission Spectra for 2Ap-Containing Oligomers. The emission spectra of 3′-2Ap ssDNA oligomers, dsDNA duplexes, and ssDNA oligomers and dsDNA duplexes with oxidized photolyase were measured with excitation at 317 nm. The spectra are shown in Figure 3 [the corresponding 5′-2Ap spectra were published by Christine et al. (*22*)]. These spectra were obtained from buffered samples consisting of 0.25 μM 3′-2Ap (—), 0.25 μM 3′-2Ap and 0.35 μM T-T oligo (- - -), 0.25 μM 3′-2Ap and 0.35 μM CPD (•••), 0.25

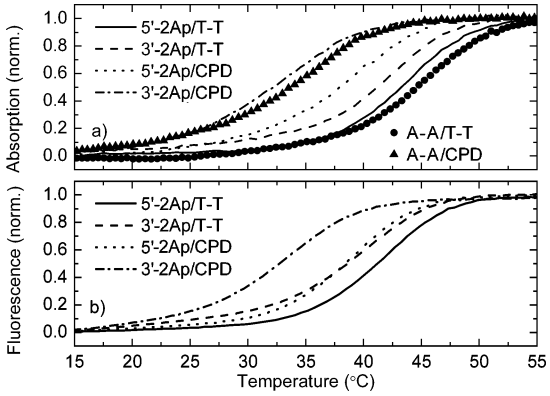

FIGURE 2: (a) Melting curves of 2Ap-containing duplexes as determined by UV−vis absorption spectroscopy. Curves plotted with symbols show the melting behavior of non-2Ap control duplexes. (b) Melting curves of 2Ap-containing duplexes as determined by fluorescence emission spectroscopy ($\lambda_{ex} = 317$ nm).

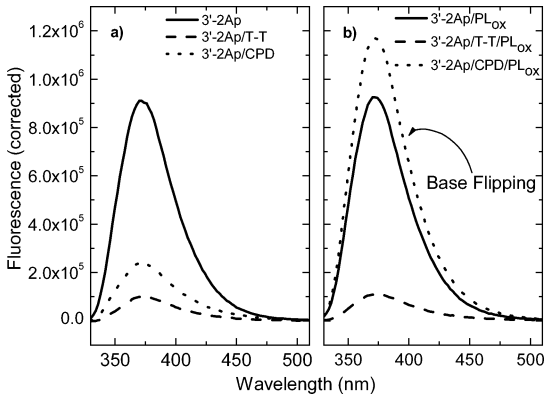

FIGURE 3: Fluorescence spectra of 3′-2Ap-containing oligos at 15 °C ($\lambda_{ex} = 317$ nm): (a) single-stranded 3′-2Ap 11-mer (—), 3′-2Ap/T-T duplex (- - -), and 3′-2Ap/CPD duplex (•••) and (b) 3′-2Ap/PL_{ox} (—), 3′-2Ap/T-T/PL_{ox} (- - -), and 3′-2Ap/CPD/PL_{ox} (•••). The salt concentration was 150 mM. The intensity of the 3′-2Ap/CPD/PL_{ox} complex is even higher than that of the 3′-2Ap/PL_{ox} control, suggesting a strong distortion of the duplex around the CPD.

μM 3′-2Ap and 0.40 μM PL_{ox} (—), 0.25 μM 3′-2Ap, 0.35 μM T-T, and 0.40 μM PL_{ox} (- - -), and 0.25 μM 3′-2Ap, 0.35 μM CPD, and 0.40 μM PL_{ox} (•••). A spectrum of 0.40 μM PL_{ox} was also obtained (data not shown). This control was subtracted from the spectra for those samples containing PL_{ox} to remove protein fluorescence and Raman scattering. Each spectrum is the average of three or more separate preparations. A quantitative analysis of the 3′-2Ap- and 5′-2Ap-containing oligonucleotides with and without PL_{ox} is presented in Table 3. The integrated fluorescence of the duplexes and ssDNA are given, as well as the emission maxima.

The fluorescence of the 3′-2Ap-containing oligo was strongly quenched when annealed to its complementary sequence (3′-2Ap/T-T). The fluorescence intensity of the CPD-containing duplex (3′-2Ap/CPD) was higher than that of the nonlesion duplex, indicating some disruption of base stacking in the CPD-containing duplex, in qualitative agreement with the melting point measurements. The emission spectra of the 3′-2Ap/T-T duplex and the 3′-2Ap/T-T/PL_{ox} control combinations were nearly identical. This indicates that the T-T-containing duplex is not effectively bound by PL_{ox}. In addition, PL_{ox} does not quench the fluorescence of 3′-2Ap-containing single-stranded DNA (3′-2Ap/PL_{ox}). This control experiment gave the expected result, indicating that PL_{ox} does not quench the 2Ap probe by nonspecific binding of this single-stranded nonsubstrate sequence. It is worth noting that these results mirror those obtained for the 5′-2Ap system in our previous study, although the 3′-2Ap probe has roughly 3 times the relative fluorescence quantum yield (as referenced to the single-stranded probe oligo) compared to the 5′-2Ap probe. This is discussed further below.

The integrated fluorescence emission of the 3′-2Ap/CPD/PL_{ox} complex was significantly higher than that of the 3′-2Ap/PL_{ox} control, while the fluorescence intensity of the 5′-2Ap/CPD/PL_{ox} complex was approximately the same as that of the 5′-2Ap/PL_{ox} control. A comparison of the integrated emission from the 3′-2Ap/CPD/PL_{ox} to 5′-2Ap/CPD/PL_{ox} complex shows that the emission quantum yield of the former is increased by a factor of ~4.4 relative to that of the latter complex. This suggests a much larger structural perturbation of the duplex at the 5′-side of the lesion compared to the 3′-side of the CPD. However, this result has to be interpreted with regard to the modulation of the fluorescence quantum yield with sequence.

In general, the fluorescence emission from the 3′-2Ap-containing duplexes was 2−4-fold higher than that of the corresponding 5′-2Ap-containing duplexes. However, while the quantum yield of the 5′-2Ap/CPD/PL_{ox} complex is approximately the same as that of 5′-2Ap, the quantum yield of the 3′-2Ap/CPD/PL_{ox} complex was greater than its single-stranded counterpart.

The emission maxima of the 3′-2Ap and 5′-2Ap systems are given in Table 3. It has been shown that a shorter emission wavelength generally correlates with better stacking and less solvent exposure (*17*). Generally, the 2-aminopurine at the 5′-side of the oligo has a slightly lower emission maximum than the 3′-case. Conversely, introduction of a CPD-containing strand shifts the emission maximum to the red by a few nanometers, suggesting an increased solvent accessibility. However, the differences are small enough that a detailed analysis appears to be inappropriate.

It is worth noting that our attempts to observe fluorescence resonance energy transfer from 2Ap* to FAD_{ox} were unsuccessful. The 370 nm emission of 2Ap overlaps well with the 370 nm absorption band ($S_0 \rightarrow S_2$) of FAD_{ox}. We have performed calculations that suggest that energy transfer between 2Ap* and FAD_{ox} is relatively inefficient, but a description of these results is deferred (K. Yang and R. J. Stanley, manuscript in preparation).

DISCUSSION

Thermostability of Probe- and Lesion-Containing Double Helices. Melting points for 2Ap-containing duplexes (*33*) or for CPD-containing duplexes have been determined by several laboratories (*31*, *34*). However, the effect on the thermostability of a combination of the fluorescent probe and CPD has not received much attention beyond our previous efforts. As assessed by UV−vis spectroscopy, the introduction of a CPD lowers the global melting point significantly (from 45 to 37 °C). This result is consistent with that obtained for a dodecamer from Jing et al., where T_m values for the control and CPD-containing duplexes were 44 and 39 °C, respectively, at 250 mM NaCl with an f_{GC} of 0.24 (*31*). Enthalpies were also reported, with values of

Table 3: Emission Maxima, Integrated Fluorescence Emission from 330 to 510 nm of 2Ap-Containing Oligonucleotides with and without PL_{ox}

sample	3′-2Ap* λ_{max} (nm)	∫3′-2Ap* ($\pm\sigma$) ($\times10^{-6}$)	normalized to ∫(3′-2Ap*/T-T)	5′-2Ap*[a] λ_{max} (nm)	∫5′-2Ap* ($\pm\sigma$) ($\times10^{-6}$)	normalized to ∫(5′-2Ap*/T-T)
probe	372	53 (0.1)	9.1 (0.4)	368	16 (0.5)	5.0 (1.5)
probe/T-T	372	5.8 (0.1)	1	368	3.2 (0.22)	1
probe/CPD	374	15 (1.1)	2.6 (0.5)	374	6.1 (0.1)	1.9 (0.5)
probe/PL_{ox}	372	55 (0.1)	9.5 (0.3)	368	16 (0.3)	5.0 (1.6)
probe/T-T/PL_{ox}	372	7.0 (0.1)	1.2 (0.1)	370	5.1 (2.1)	1.6 (0.1)
probe/CPD/PL_{ox}	374	70 (0.2)	12.1 (1.2)	368	16 (0.3)	5.0 (1.7)

[a] The fluorescence data of 5′-2Ap-containing oligos with and without PL_{ox} were adapted from our previous paper and then adjusted to the concentrations used in this study for comparison.

−79.8 and −75.1 kcal/mol at 37 °C, respectively. Our values are somewhat higher (−94 and −82 kcal/mol, respectively), which is probably due to the much higher GC content (f_{GC}) of the oligos used in this study ($f_{GC} = 0.55$).

The replacement of adenine with 2Ap leads to a decrease in the T_m, as expected. The slight difference in the melting points due to the position of the probe suggests that sequence plays a role in stabilizing the modified base in the double helix. This sequence dependence may be due to differences in base stacking stability, as reported by others (*35*). This would suggest that the nearest-neighbor free energies (5′−3′/3′−5′) for CA−GT ($\Delta G° = -1.45$ kcal/mol) and AC−TG ($\Delta G° = -1.44$ kcal/mol) should be different to account for the difference in melting temperatures, but they are not ($\Delta\Delta G° = -0.01$ kcal/mol). To our knowledge, however, the free energies for nearest-neighbor interactions with 2Ap (e.g., C2Ap−GT) are not known and may result in a $\Delta\Delta G$ larger than that for adenine. More significantly, 2Ap and adenine will display different hydrogen bonding patterns with the complementary strand. To our knowledge, there have been no reports of 2-aminopurine/DNA duplex crystal structures. Without structural evidence, it is difficult to assess the significance of this conjecture.

Interestingly, the introduction of the CPD in the 5′-2Ap case leads to a T_m slightly higher than that of the control duplex, which is considerably more stable than the 3′-2Ap/CPD duplex. This is also reflected by the difference between the fluorescence intensity of the CPD-containing duplex and the perfectly matched duplex. The fluorescence intensity of the CPD-containing duplex is greater than that of the perfectly matched duplex, which indicates that the CPD destabilizes base stacking locally. It is possible that the 2-amino group of the 2Ap forms stronger hydrogen bonds with the CPD than adenine does, given the structural perturbation of the CPD relative to the undamaged thymine pair. The crystal structure shows that the 5′-adenine (in the sense used in this work) is most perturbed, with the hydrogen bond distance growing to ∼2.5 Å, compared to 1.9 Å for the 3′-adenine (*30*). This distortion of base pairing may be compensated by the 2-amino group of the 5′-2Ap, but this is only conjecture.

The modest increase in the emission of the CPD-containing duplex relative to that of the T-T-containing duplex is consistent with the CPD-containing decamer duplex crystal structures of Park et al. (*30*), which show that the structural disruption of the CPD-containing strand is not echoed by the complementary adenines across the helix. However, the 3′-adenine does lose some hydrogen bonding with the 5′-side of the CPD, which is consistent with the red shift observed for the 3′-2Ap probe. The emission maxima of the 5′-2Ap duplexes are slightly blue shifted compared to their 3′-2Ap counterparts. This supports the melting point data and suggests that the 2Ap base may be less solvent exposed than the 3′-2Ap systems.

It is worth pointing out the underlying assumption of a two-state model for the calculation of van't Hoff enthalpies implicit in our work and in the cited studies. If the melting process includes intermediates other than folded and unfolded states, then the analysis of Breslauer is inappropriate. The presence of more than two states can be ascertained by obtaining melting data as a function of concentration or by using an alternate method, such as calorimetry (*35*, *36*). It would be of great interest to see the results of such studies so that the fluorescence and absorption data can be better understood.

Sequence Dependence of the Fluorescence Quantum Yield. The fluorescence intensity of the 3′-probe oligo is always higher than that of the 5′-probe oligo for both single-stranded oligos and duplexes. For example, the single-stranded 3′-2Ap and 5′-2Ap oligos are different in only the position of the 2Ap. However, the ratio of their integrated intensities is ∼3.3. This modulation of quantum yield depends on interactions of the probe with its neighbors, which has been documented in other systems (*37*). When 3′-2Ap and 5′-2Ap are compared, the adjacent bases in 3′-2Ap are adenine at the 5′-side and cytosine at the 3′-side (A-2Ap-C). The bases adjacent to 5′-2Ap are cytosine at the 5′-side and adenine at the 3′-side (C-2Ap-A).

Electron transfer between DNA bases and 2Ap* is possible and is considered to be the source of sequence-dependent quantum yields observed in these systems (*38*). The oxidation potentials of 2Ap* and the normal DNA bases G, A, C, and T are 1.5, 1.3, 1.4, 1.6, and 1.7 V versus the normal hydrogen electrode, respectively (*39*−*41*). On the basis of these oxidation potentials, the oxidation of guanine by 2Ap* is most facile while the oxidation of thymine is least likely. However, thymine can be reduced by an electron transfer reaction from 2Ap* (*42*). The rate constant for electron transfer to or from the excited base analogue will depend exponentially on the driving force for oxidation of purine bases (G and A) or reduction of pyrimidine bases (T and C), respectively. The smaller this driving force, the smaller the degree of fluorescence quenching. This effect has been documented in 2Ap* (G < A; T < C) (*41*, *43*).

However, electron transfer is not required to rationalize the sequence dependence of the fluorescence quantum yield. Calculations show that charge transfer states are engendered when 2Ap enters into base stacking (*37*). In contrast to the case cited above, these states do not involve complete electron transfer to explain quenching. Instead, a partial

separation of charge across the supramolecular complex is invoked. Ultrafast internal conversion from the Franck−Condon state obtained upon absorption of light to a dark charge transfer (CT) state will lead to fluorescence quenching as well, as CT states will often decay nonradiatively (*44*).

Another potential source of reduced fluorescence is a reduction in oscillator strength for the probe due to base stacking interactions. This change in extinction coefficient was identified by TDDFT calculations of stacking interactions in a model trimer consisting of 2Ap flanked by either pyrimidines or purines (*44*). The calculations show that the electronic interaction of 2Ap with neighboring pyrimidines does not affect the oscillator strength of the probe. However, if 2Ap is flanked by purine, the electronic effect of a 3′-purine is different from that of a 5′-side purine. In a 5′-2Ap-G-3′ dinucleotide, the oscillator strength of the 2Ap is approximately half of that of the 2Ap without flanking bases, but in a 5′-G-2Ap-3′ dimer, the oscillator strength is similar to that of the 2Ap monomer. Our results corroborate this prediction, at least semiquantitatively. The emission intensity ratio for the 3′-2Ap/5′-2Ap ssDNA oligo is 3.3. In dsDNA, the (3′-2Ap/T-T)/(5′-2Ap/T-T) emission intensity ratio is 1.8. However, our experiments do not allow the contribution to static quenching to be separated from the CT component.

Structural Considerations. Biochemical investigations into the structural requirements for CPD binding by photolyase revealed the importance of DNA backbone contacts made by the substrate with the protein binding pocket (*45*). Methylation of the substrate strand showed that PL protects two phosphodiester bonds on the 5′-side of the CPD and two or three phosphodiester bonds on the 3′-side, with weaker contacts made with the complementary strand. Interestingly, these studies did not suggest base flipping as a necessary requirement for substrate binding. This hypothesis was formed when the first crystal structure was determined, showing a cavity with dimensions sufficient to accommodate the CPD in the proximity of the FAD (*19*).

While our experiments were in progress, a crystal structure was published that gives a picture of *Anacystis nidulans* photolyase bound to a modified DNA duplex (*26*). A CPD with a formacetal backbone linkage was used to improve the probability of obtaining diffraction-quality crystals. The structure showed that the cyclobutane ring had been repaired but that the monomeric thymidines remain tucked neatly into the substrate pocket of the protein, confirming the base flipping hypothesis (*19*, *21*, *22*). Significantly for this study, the complementary strand was well-resolved (see Scheme 2, constructed from PDB entry 1TEZ).

As substantiated by our results, present and prior, the complementary strand is completely disrupted between the two adenines that complement the CPD. The top part of the scheme represents the complementary strand, with the (lighter) interior adenines flanked by the (darker) adjacent guanine bases. The CPD is shown in the bottom part of the scheme. All other bases and the protein have been removed for clarity.

Each complementary adenine is within ~3.5 Å of the adjacent guanine. In the case of the 5′-adenine, base stacking appears to be preserved on its 5′-side with a complete loss of stacking at the 3′-side. The 3′-adenine is exposed to the solvent at its 5′-side and appears to stack with the complementary 3′-guanine. However, closer inspection shows that these bases are rotated significantly compared to the B-form DNA helical structure. This structural difference may provide a clue about why the 3′-2Ap fluorescence quantum yield is much larger than its 5′-counterpart. A loss of π-orbital overlap due to this rotation will further attenuate any of the interactions cited above.

Scheme 2

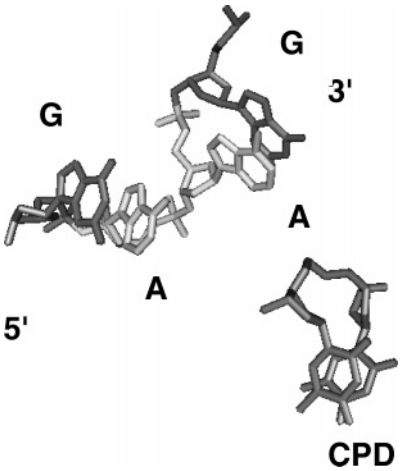

Importantly, our results show that this structural perturbation is found in solution as well as in the crystal structure. The most straightforward interpretation of this study is that the 5′-side of the CPD is highly disordered and that the 3′-2Ap probe experiences less base stacking when substrate is bound to the protein than when it is in ssDNA. This is corroborated by the crystal structure. In this study, however, the substantial differential response of the 2AP probe may be due, in part, to the lower stability of the 3′-2Ap/CPD duplex, as evidenced by both fluorescence- and absorption-based melting point data.

Clearly, the fluorescent adenine analogue 2Ap is a highly sensitive structural probe, but changes in its fluorescence yield may depend on quite subtle structural features. This sensitivity can be exploited in carefully designed experiments to study the dynamics of substrate binding by photolyase, as well as other DNA-binding proteins. However, more insight into the detailed quenching mechanism is required before 2Ap (and other fluorescent base analogues) can be exploited fully in this context.

REFERENCES

1. Taylor, J. S. (1994) Unraveling the Molecular Pathway from Sunlight to Skin Cancer, *Acc. Chem. Res. 27*, 76−82.
2. Sancar, A. (1994) Structure and Function of DNA Photolyase, *Biochemistry 33*, 2−9.
3. Cadet, J., and Vigny, P. (1990) The Photochemistry of Nucleic Acids, in *Bioorganic Chemistry* (Morrison, H., Ed.) pp 1−272, Wiley, New York.
4. Yoon, J. H., Lee, C. S., O'Connor, T. R., Yasui, A., and Pfeifer, G. P. (2000) The DNA damage spectrum produced by simulated sunlight, *J. Mol. Biol. 299*, 681−93.
5. You, Y.-H., Lee, D.-H., Yoon, J.-H., Nakajima, S., Yasui, A., and Pfeifer, G. P. (2001) Cyclobutane pyrimidine dimers are responsible for the vast majority of mutations induced by UVB irradiation in mammalian cells, *J. Biol. Chem. 276*, 44688−94.
6. Begley, T. P. (1994) Photoenzymes: A Novel Class of Biological Catalysts, *Acc. Chem. Res. 27*, 394−401.
7. Vassylyev, D. G., Kashiwagi, T., Mikami, Y., Ariyoshi, M., Iwai, S., Ohtsuka, E., and Morikawa, K. (1995) Atomic model of a

pyrimidine dimer excision repair enzyme complexed with a DNA substrate: Structural basis for damaged DNA recognition, *Cell 83*, 773−82.
8. Sharova, N. P. (2005) How does a cell repair damaged DNA? *Biochemistry (Moscow) 70*, 275−91.
9. Reardon Joyce, T., and Sancar, A. (2003) Recognition and repair of the cyclobutane thymine dimer, a major cause of skin cancers, by the human excision nuclease, *Genes Dev. 17*, 2539−51.
10. Sancar, A. (2003) Structure and function of DNA photolyase and cryptochrome blue-light photoreceptors, *Chem. Rev. 103*, 2203−37.
11. Jorns, M. S., Sancar, G. B., and Sancar, A. (1984) Identification of a neutral flavin radical and characterization of a second chromophore in *Escherichia coli* DNA photolyase, *Biochemistry 23*, 2673−9.
12. Kim, S. T., Heelis, P. F., Okamura, T., Hirata, Y., Mataga, N., and Sancar, A. (1991) Determination of rates and yields of interchromophore (folate → flavin) energy transfer and intermolecular (flavin → DNA) electron transfer in *Escherichia coli* photolyase by time-resolved fluorescence and absorption spectroscopy, *Biochemistry 30*, 11262−70.
13. Langenbacher, T., Zhao, X. D., Bieser, G., Heelis, P. F., Sancar, A., and Michel Beyerle, M. E. (1997) Substrate and temperature dependence of DNA photolyase repair activity examined with ultrafast spectroscopy, *J. Am. Chem. Soc. 119*, 10532−6.
14. MacFarlane, A. W., IV, and Stanley, R. J. (2003) Cis-syn thymidine dimer repair by DNA photolyase in real time, *Biochemistry 42*, 8558−68.
15. Kao, Y.-T., Saxena, C., Wang, L., Sancar, A., and Zhong, D. (2005) Direct observation of thymine dimer repair in DNA by photolyase, *Proc. Natl. Acad. Sci. U.S.A. 102*, 16128−32.
16. Roberts, R. J. (1995) On Base Flipping, *Cell 82*, 9−12.
17. Allan, B. W., and Reich, N. O. (1996) Targeted base stacking disruption by the EcoRI DNA methyltransferase, *Biochemistry 35*, 14757−62.
18. McCullough, A. K., Dodson, M. L., Scharer, O. D., and Lloyd, R. S. (1997) The role of base flipping in damage recognition and catalysis by T4 endonuclease V, *J. Biol. Chem. 272*, 27210−7.
19. Park, H. W., Kim, S. T., Sancar, A., and Deisenhofer, J. (1995) Crystal structure of DNA photolyase from *Escherichia coli*, *Science 268*, 1866−72.
20. Butenandt, J., Burgdorf, L. T., and Carell, T. (1999) "Base flipping": Photodamaged DNA-RNA duplexes are poor substrates for photoreactivating DNA-repair enzymes, *Angew. Chem., Int. Ed. 38*, 708−11.
21. Vande Berg, B. J., and Sancar, G. B. (1998) Evidence for dinucleotide flipping by DNA photolyase, *J. Biol. Chem. 273*, 20276−84.
22. Christine, K. S., MacFarlane, A. W., IV, Yang, K., and Stanley, R. J. (2002) Cyclobutylpyrimidine Dimer Base Flipping by DNA Photolyase, *J. Biol. Chem. 277*, 38339−44.
23. Ward, D. C., Reich, E., and Stryer, L. (1969) Fluorescence Studies of Nucleotides and Polynucleotides, *J. Biol. Chem. 244*, 1228−37.
24. Allan, B. W., Beechem, J. M., Lindstrom, W. M., and Reich, N. O. (1998) Direct real time observation of base flipping by the EcoRI DNA methyltransferase, *J. Biol. Chem. 273*, 2368−73.
25. Holz, B., Dank, N., Eickhoff, J. E., Lipps, G., Krauss, G., and Weinhold, E. (1999) Identification of the binding site for the extrahelical target base in N-6-adenine DNA methyltransferases by photo-cross-linking with duplex oligodeoxyribonucleotides containing 5-iodouracil at the target position, *J. Biol. Chem. 274*, 15066−72.
26. Mees, A., Klar, T., Gnau, P., Hennecke, U., Eker, A. P. M., Carell, T., and Essen, L. O. (2004) Crystal structure of a photolyase bound to a CPD-like DNA lesion after in situ repair, *Science 306*, 1789−93.
27. Jorns, M. S., Wang, B. Y., Jordan, S. P., and Chanderkar, L. P. (1990) Chromophore function and interaction in *Escherichia coli* DNA photolyase: Reconstitution of the apoenzyme with pterin and/or flavin derivatives, *Biochemistry 29*, 552−61.
28. Banerjee, S. K., Christensen, R. B., Lawrence, C. W., and Leclerc, J. E. (1988) Frequency and Spectrum of Mutations Produced by a Single Cis-Syn Thymine-Thymine Cyclobutane Dimer in a Single-Stranded Vector, *Proc. Natl. Acad. Sci. U.S.A. 85*, 8141−5.
29. Breslauer, K. J. (1995) Extracting thermodynamic data from equilibrium melting curves for oligonucleotide order−disorder transitions, *Methods Enzymol. 259*, 221−42.
30. Park, H., Zhang, K. J., Ren, Y. J., Nadji, S., Sinha, N., Taylor, J. S., and Kang, C. H. (2002) Crystal structure of a DNA decamer containing a cis-syn thymine dimer, *Proc. Natl. Acad. Sci. U.S.A. 99*, 15965−70.
31. Jing, Y., Kao, J. F. L., and Taylor, J.-S. (1998) Thermodynamic and base-pairing studies of matched and mismatched DNA dodecamer duplexes containing cis-syn, (6−4) and Dewar photoproducts of TT, *Nucleic Acids Res. 26*, 3845−53.
32. Taylor, J. S., Garrett, D. S., Brockie, I. R., Svoboda, D. L., and Telser, J. (1990) ^{1}H NMR assignment and melting temperature study of cis-syn and trans-syn thymine dimer containing duplexes of d(CGTATTATGC)·d(GCATAATACG), *Biochemistry 29*, 8858−66.
33. Law, S. M., Eritja, R., Goodman, M. F., and Breslauer, K. J. (1996) Spectroscopic and calorimetric characterizations of DNA duplexes containing 2-aminopurine, *Biochemistry 35*, 12329−37.
34. McAteer, K., Jing, Y., Kao, J., Taylor, J. S., and Kennedy, M. A. (1998) Solution-state structure of a DNA dodecamer duplex containing a cis-syn thymine cyclobutane dimer, the major UV photoproduct of DNA, *J. Mol. Biol. 282*, 1013−32.
35. SantaLucia, J., Jr., and Hicks, D. (2004) The thermodynamics of DNA structural motifs, *Annu. Rev. Biophys. Biomol. Struct. 33*, 415−40.
36. Petersheim, M., and Turner, D. H. (1983) Base-stacking and base-pairing contributions to helix stability: Thermodynamics of double-helix formation with CCGG, CCGGp, CCGGAp, ACCGGp, CCGGUp, and ACCGGUp, *Biochemistry 22*, 256−63.
37. Jean, J. M., and Hall, K. B. (2004) Stacking−unstacking dynamics of oligodeoxynucleotide trimers, *Biochemistry 43*, 10277−84.
38. Wan, C. Z., Fiebig, T., Schiemann, O., Barton, J. K., and Zewail, A. H. (2000) Femtosecond direct observation of charge transfer between bases in DNA, *Proc. Natl. Acad. Sci. U.S.A. 97*, 14052−5.
39. Kelley, S. O., and Barton, J. K. (1999) Electron transfer between bases in double helical DNA, *Science 283*, 375−81.
40. Steenken, S., and Jovanovic, S. V. (1997) How easily oxidizable is DNA? One-electron reduction potentials of adenosine and guanosine radicals in aqueous solution, *J. Am. Chem. Soc. 119*, 617−8.
41. Larsen, O. F. A., van Stokkum, I. H. M., de Weerd, F. L., Vengris, M., Aravindakumar, C. T., van Grondelle, R., Geacintov, N. E., and van Amerongen, H. (2004) Ultrafast transient-absorption and steady-state fluorescence measurements on 2-aminopurine substituted dinucleotides and 2-aminopurine substituted DNA duplexes, *Phys. Chem. Chem. Phys. 6*, 154−60.
42. Fiebig, T., Wan, C. Z., and Zewail, A. H. (2002) Femtosecond charge transfer dynamics of a modified DNA base: 2-Aminopurine in complexes with nucleotides, *ChemPhysChem 3*, 781−8.
43. Somsen, O. J. G., Hoek, V. A., and Amerongen, V. H. (2005) Fluorescence quenching of 2-aminopurine in dinucleotides, *Chem. Phys. Lett. 402*, 61−5.
44. Jean, J. M., and Hall, K. B. (2002) 2-Aminopurine electronic structure and fluorescence properties in DNA, *Biochemistry 41*, 13152−61.
45. Husain, I., and Sancar, A. (1987) Binding of *Escherichia coli* DNA photolyase to a defined substrate containing a single T<>T dimer, *Nucleic Acids Res. 15*, 1109−20.

BI060408U